Global Journal of Researches in Engineering: J General Engineering
Volume 22 Issue 2 Version 1.0 Year 2022
Type: Double Blind Peer Reviewed International Research Journal
Publisher: Global Journals
Online ISSN: 2249-4596 & Print ISSN: 0975-5861

CO_2-Foam Monitoring using Resistivity and Pressure Measurements

By Metin Karakas, Fred Aminzadeh & Arne Graue
University of Bergen

Abstract- This paper focuses on combining resistivity and pressure measurements to determine the effectiveness of foam as a mobility control method. It presents a theoretical framework to describe the expected resistivity changes during CO_2-foam displacements. With this objective, we first provide equations to estimate the resistivity for CO_2-foam systems and then utilize two distinct foam models to quantify these effects. Using analytical solutions based on the fractional flow theory, we present resistivity and mobility distributions for ideal and non-ideal reservoir displacement scenarios. Additionally, assuming pressure measurements only, we examine the inter-dependency between various foam parameters. Our results suggest that the combination of pressure and resistivity measurements in time-lapse mode could be deployed as an effective monitoring tool in field applications of the (CO_2) foam processes. The proposed method is novel as it could be employed to predict under-performing CO_2-foam floods and improve oil recovery and CO_2 storage.

GJRE-J Classification: DDC Code: 620 LCC Code: TP1183.F6

Strictly as per the compliance and regulations of:

CO_2-Foam Monitoring using Resistivity and Pressure Measurements

Metin Karakas [α], Fred Aminzadeh [σ] & Arne Graue [ρ]

Abstract- This paper focuses on combining resistivity and pressure measurements to determine the effectiveness of foam as a mobility control method. It presents a theoretical framework to describe the expected resistivity changes during CO_2-foam displacements. With this objective, we first provide equations to estimate the resistivity for CO_2-foam systems and then utilize two distinct foam models to quantify these effects. Using analytical solutions based on the fractional flow theory, we present resistivity and mobility distributions for ideal and non-ideal reservoir displacement scenarios. Additionally, assuming pressure measurements only, we examine the inter-dependency between various foam parameters. Our results suggest that the combination of pressure and resistivity measurements in time-lapse mode could be deployed as an effective monitoring tool in field applications of the (CO_2) foam processes. The proposed method is novel as it could be employed to predict under-performing CO_2-foam floods and improve oil recovery and CO_2 storage.

I. Introduction

Time-lapse seismic, resistivity, electromagnetic (EM), and pressure measurements have been used in the oil industry for water and CO_2 flooding and monitoring applications. For example, see: Passalacqua et al (2018), Davydycheva and Strack (2018) and Strack(2014). CO_2 foam injection is an effective method to control mobility during CO_2-Enhanced Oil Recovery processes in petroleum reservoirs. When it is done optimally, CO_2 foam can improve sweep efficiency, oil production, and CO_2 storage (Kuuskraaet al., 2006, Fernoet al., 2014). Laboratory studies show that foam strength is essential to achieve the desired reservoir efficiency. It has been demonstrated that the foam density is a direct function of the density of the lamellae (Kovscek and Radke, 1994). Additionally, the solubility of surfactant in CO_2 and water phases, as well as the adsorption of CO_2 on the rock, play a crucial role in these displacements. At a given reservoir temperature, the partitioning of the CO_2 soluble surfactants is dependent on pressure and strongly influenced by the attractiveness (CO_2-philicity) of the selected surfactant for foam application. Recent research indicates that various (cationic, nonionic, and zwitterionic) surfactants as the leading candidates for CO_2 foams. It is also critical to maintaining the foam strength for the entire injection period during reservoir applications. Additionally, the CO_2 mobility is higher than that of the foam, and under certain conditions, this can lead to less-than-optimal displacement in porous media.

Foam monitoring has been restricted to electrokinetic (streaming potential) measurements (Omar et al., 2013). Wo et al. (2012) ran foam experiments on unsaturated soil samples and investigated the possibility of using electrical measurements for foam monitoring. Of course, it should be realized that foam and CO_2 are charged. They connect and eventually build larger molecules. We need boundary to develop a bouble layer for charges to collect. Wo et al. (2012) reported significant changes in electrical properties with foam formation.

Karakas and Aminzadeh (2017) proposed time-lapse measurements with an array of permanently deployed sensors to detect the movement of the foam-CO_2-Oil interface in the reservoir due to CO_2-foam injection. With the proposed method, resistivity and pressure measurements are acquired simultaneously during the CO_2-foam Injection into reservoir, as shown in Fig. 1.

Author α ρ: University of Bergen, Norway.
Author σ: FACT Inc., United States. e-mail: metin.karakas@uib.no

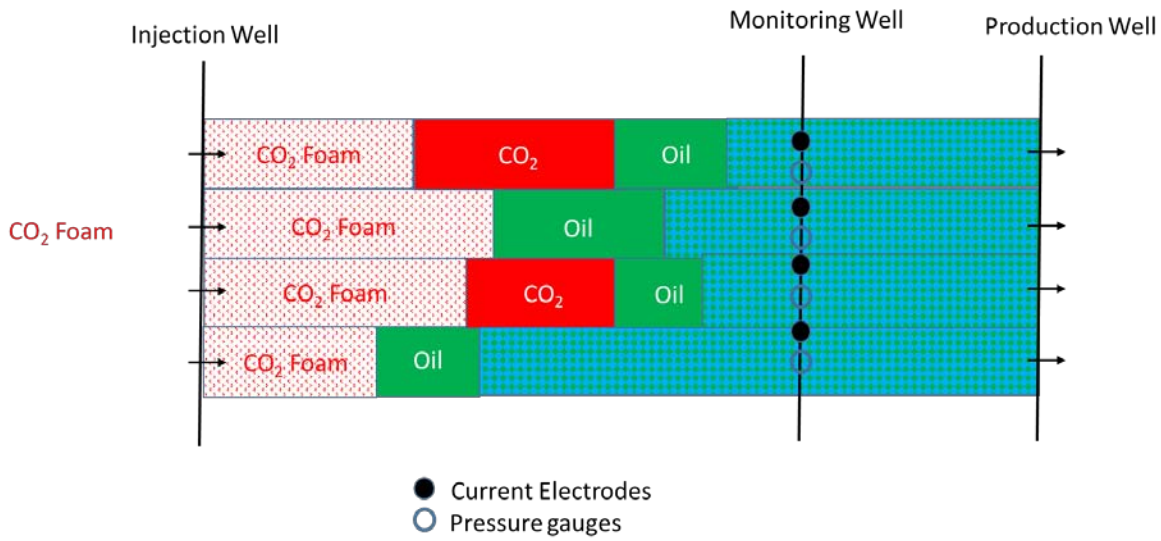

Fig. 1: Example of pressure and resistivity monitoring during a CO_2 Foam flood (Karakas and Aminzadeh, 2017).

In the proposed method by Karakas and Aminzadeh (2017), resistivity and pressure measurements are used to determine the effectiveness of foam as a mobility control method and hence, provide a way to remedy any under-performing foam (and CO_2-foam) floods to improve both oil recovery and CO_2 storage. This monitoring is crucial for applying foam (and CO_2 foam) in reservoirs where heterogeneity is involved. Figure 2 below illustrates this optimization process.

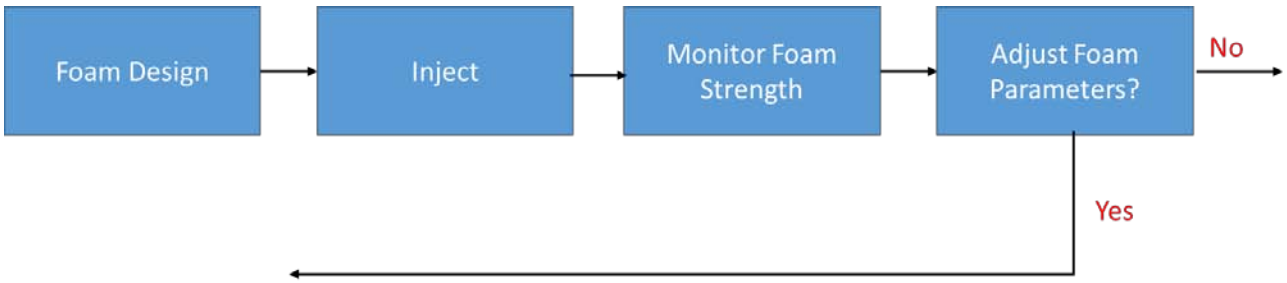

Fig. 2: Foam (and CO_2-Foam) optimization process (Karakas and Aminzadeh, 2017).

In terms of laboratory studies, Berge (2017) conducted resistivity measurements while injecting CO_2 and surfactant solution into saturated cores and Haroun et al. (2017) monitored resistivity and pressure changes during foam generation in the formation-brine saturated carbonate core plug samples. Haroun et al. (2017) reported significant increases in resistivity and pressure with foam development.

The main thrust of this paper is to the characterize the resistivity response and to present a theoretical foundation for resistivity monitoring during CO_2 foam displacements.

II. CO_2 Foam Transport Modeling

The transport of CO_2 foam can be described by several methods (Ma, K. et al., 2015). These include:

- Pore-network models
- Analytical methods
- Explicit population-based equation (PBE) methods
- Implicit foam methods

Pore-Network models provide a good insight into foam transport and are not yet practical for reservoir-scale applications. In this study, we focus on the Analytical and the explicit (or Population Based) methods. The analytical approach is based on the fractional-flow theory and steady-state foam development, as presented by Ashoori et al. (2010). The main assumptions are as follows:

- One-dimensional flow.
- Initially, the reservoir is at residual oil saturation (S_{or}) after waterflooding.
- CO_2 is injected at supercritical conditions.
- First-Contact Miscible (FCM) displacement of oil by the injected supercritical CO_2.
- The relative permeability depends on water saturation and the oil or CO_2 saturations.
- Foam effects are captured implicitly using steady-state assumption.

As demonstrated by Ashoori et al. (2010), there are two different solutions: the first one relates to an

ideal CO_2-foam displacement where the miscible (CO_2) and surfactant (foam) fronts travel at the same speed. In this case, three separate banks develop in the reservoir: Foam or surfactant (CO_2 plus water) bank, oil (with mobile water) bank, and water (with residual oil) bank. The second solution assumes a non-ideal CO_2-foam displacement. In this case, due to adsorption of the injected surfactant to the rock and its partitioning to the water phase, the foam front slows down, and the miscible (CO_2) front moves ahead of it. In this case, a separate CO_2 bank forms ahead of the foam (or surfactant) bank, which gives rise to an unfavorable mobility distribution in the reservoir. These reconstructed saturation profiles are provided in Appendix A. The fractional flow approach is based on the steady-state assumption and cannot capture the transient foam development during CO_2 foam injection (Kam S.I.,2008).

III. Population-Balance Method

In the Population Based (PBE) method, foam effects are captured explicitly by quantifying the bubble population (n_f) and correlating it to the foam mobility. In this work, we utilized the solution approach provided by Kam and Rossen (2003). The relevant foam equations are provided in Appendix B. Please note that this solution is based on the two-phase (CO_2 and water) flow, and the oil phase is ignored. This assumption is in line with most experimental work and gives good insight into foam development in porous media (Kam et al., 2004, Prigiobbe et al., 2016).

The solution of the PBE, due to nonlinear relations between injection rate and pressure gradient, is quite complex and may not be unique (Dholhawala, Z.F. et al., 2007). In this work, a numerical approach was taken for solving the transient foam equations. With this objective, a numerical foam simulator (FoamSim) was developed, in which upstream weighting was utilized to minimize the numerical dispersion effects. The numerical model was validated by comparing its results with that of Kam et al. (2004). These comparisons were made for both weak and strong foam states.

IV. Parameter Estimation using Pressure Measurements

One of the crucial considerations is the uniqueness of the model parameters obtained from pressure measurements. For this reason, we analyzed the inter dependency between various foam parameters. These included foam generation parameters (C_g & m), foam coalescence parameters (C_c& n), and the foam viscosity parameter (C_f). For this purpose, we utilized the published CO_2foam experiments by Prigiobbe et al. (2016). The foam parameters for these history matched experiments are as follows:

Table 1: Model Parameters used for Foam Simulations (From Prigiobbe et al., 2016).

	C_f	C_g	C_c	M	n	S_w*
Experiment 6	1.58E-15	3.02E+07	3.02E-01	0.588	0.73	0.121
Experiment 34	3.31E-17	3.72E+06	9.55E-03	1.140	0.29	0.01

We first ran forward simulations using FoamSim and compared our results with those of Prigiobbe et al. Two experiments (6 & 34) produced very similar (but not exact) results. The graph below shows the comparison for Experiment 6 using parameters from the table above.

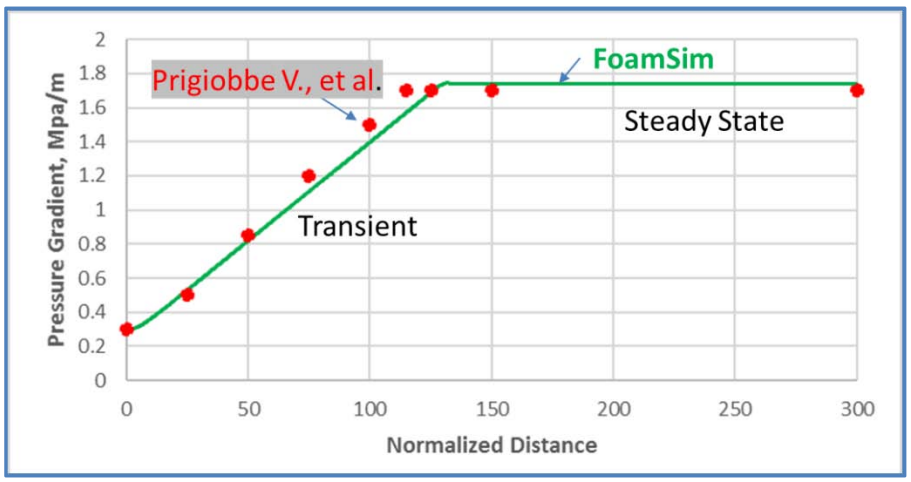

Fig. 3: Comparison of pressure gradients (experiment number 6).

The relevant sensitivity coefficients were generated using our numerical solver (FoamSim), and for experiments 6 and 34 and the duration of the lab experiments. In this analysis, the following parameters were considered:

$$X = \text{foam parameters } [C_g, C_c, C_f, m, n] \quad (1)$$

For most high-permeability systems, the critical water saturation (S_w^*) is relatively small. Therefore, due to potential numerical problems, it was not included in the analysis. In the calculations of sensitivity coefficients, we used the log transformation for all the foam parameters:

$$C_g' = \log_{10}(C_g) \quad (2)$$

The following plot shows the calculated sensitivity coefficients using data from experiment number 6:

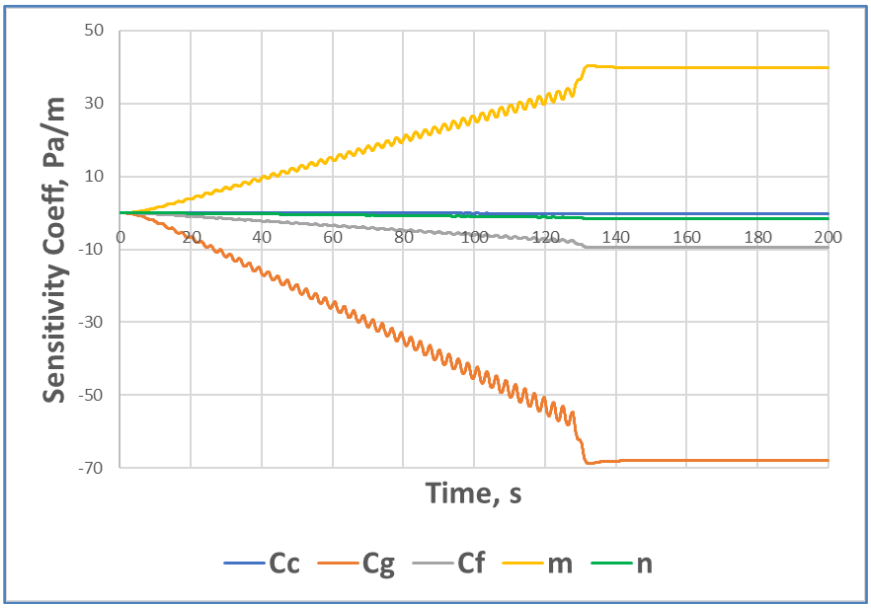

Fig. 4: Sensitivity coefficients for foam parameters (experiment number 6).

We also normalized sensitivity coefficients for an even comparison and calculated the determinant of the sensitivity matrix to examine the (ill) conditioning of the inverse problem. The determinant (d) is a function of time and is defined as follows:

$$d = [S^T S] \quad (3)$$

These calculations showed that the magnitude of the determinant increased with time (with more measurement samples):

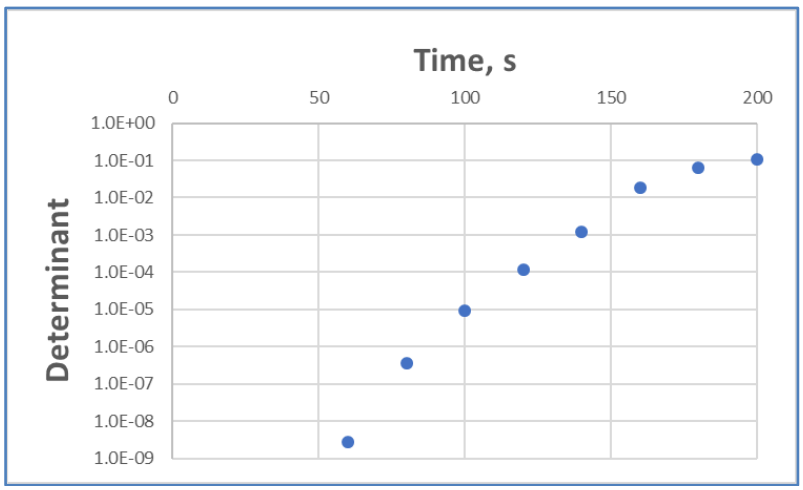

Fig. 5: Determinant of the sensitivity matrix.

We also calculated the determinant using the steady-state portion of the measurements only. For steady-state flow, the determinant became very small, which indicates a linear dependency between the selected foam parameters (Appendix B). This examination showed the following:

- Foam generation parameters, C_g & m, have by far the highest sensitivity.
- Foam viscosity coefficient, C_f, is of the middle rank.
- Foam coalescence parameters, C_c & n, have relatively less sensitivity.
- Linear independence is possible with transient data.
- Steady-State pressure measurements give rise to an ill-conditioned parameter estimation problem and the grouping of parameters is necessary.

V. CO_2 Foam Resistivity Characteristics and Modeling

Typically, nonionic surfactants are dissolved in the CO_2 phase, and the foam generation occurs in situ when injected the CO_2 plus surfactant meets the formation brine. CO_2 is highly resistive, whereas the thin water film is conductive (depending on the salinity of the in-situ reservoir fluid). During foam injection, these films enhance the electrical conductivity. With growing bubble size, these conduits become less effective, and overall, the resistivity of the foam system increases. However, with CO_2 injected brine already resistive this will only produce more resistive fluid. Reduction in resistivity will come from higher electron flow and resistivity reduction caused by pressure changes. See Boerner et al (2015) on electrical conductivity of CO_2-bearing pore waters at elevated pressure and temperature.

Assuming a uniform and hexagonal-prism shape foam, the foam conductivity σ_f is obtained using the Lemlich Relation (Lemlich, R., 1985):

$$K = \frac{D}{3} \tag{4}$$

Where K is the bulk foam conductivity. This relationship can also be written as follows:

$$K = \frac{\text{conductivity of dispersion}}{\text{conductivity of continous phase}} = \frac{\sigma_f}{\sigma_s} \tag{5}$$

Where D is the volumetric liquid fraction or = (1-X_f), and X_f is the foam quality. Using these relationships, we obtain:

$$\sigma_f = \frac{1}{3}\sigma_s\,(1 - X_f) \tag{6}$$

or another expression would be:

$$\sigma_f = c_1 * \sigma_s * (1\text{-}S_{co2}^f) \tag{7}$$

where:

c_1 = constant

S_{co2}^f = CO_2 saturation with foam

σ_s = conductivity of the thin film around bubbles

Assuming, σ_s = 1.0 S/m and X_f = 0.90 (foam quality), we obtain the following values for foam conductivity:

σ_f = 0.033 S/m (foam conductivity) or R_f = 30 ohm.m (foam resistivity)

These results suggest that foam conductivity will be order of (1 to 2) higher compared to that of the CO_2 phase only.

We propose to scale the foam conductivity with foam density as follows:

$$\sigma_f = c1\,\sigma_s\,(1\text{-}S_{co2}^f)\,(\frac{n_f}{n_{fmax}}) \tag{8}$$

where n_{fmax} is the maximum population density.

For a CO_2-Water system, lab results show that Archie's equation provides a reasonable approximation (Bergmannet al., 2013). Assuming a CO_2-Foam-Water system, the total system conductivity was calculated by utilizing the mixing law (Appendix D):

$$\sigma=\phi^2\,[S_{co2}^f\sigma_f^{\,1/2} + S_w\sigma_w^{\,1/2}]^{\,2} \tag{9}$$

Laboratory measurements using carbonate cores from Abu Dhabi (Harounet al., 2017) show a sharp increase in resistivity and a large pressure drop with the formation of foam during these high-temperature and high-pressure core floods. These experimental results are in line with the theoretical results provided here.

The difference between foam and CO_2 saturated reservoir depends on how much CO_2 is absorbed by the brine. However, strictly speaking, volumetrics are empirical correlations and do not often work for resistivity due to non-linearity of Archie. With fracture we increase complexity even further.

a) *Resistivity Profiles*

Using the simulated saturation and the foam densities, we can now estimate the resistivity (along with relative mobility) evolution during the CO_2-Foam displacements. For these simulations, we assumed the following bulk conductivities for water, CO_2, foam, and oil phases:

Table 2: Parameters Used For Resistivity Simulations

σ_w	5.00	S/m
σ_{CO2}	0.001	S/m
σ_f	0.100	S/m
σ_{oil}	0.001	S/m

The figure below shows the resistivity profile from one dimensional CO_2 foam flood assuming a moderately conductive water scenario. The resistivity profile has been calculated using the simulated foam densities from the FoamSim simulator, and the CO_2 foam resistivity model. To avoid using canonical resistivity values one would in practice scale the surface measurements to the borehole scale as shown by Strack et al (2022).

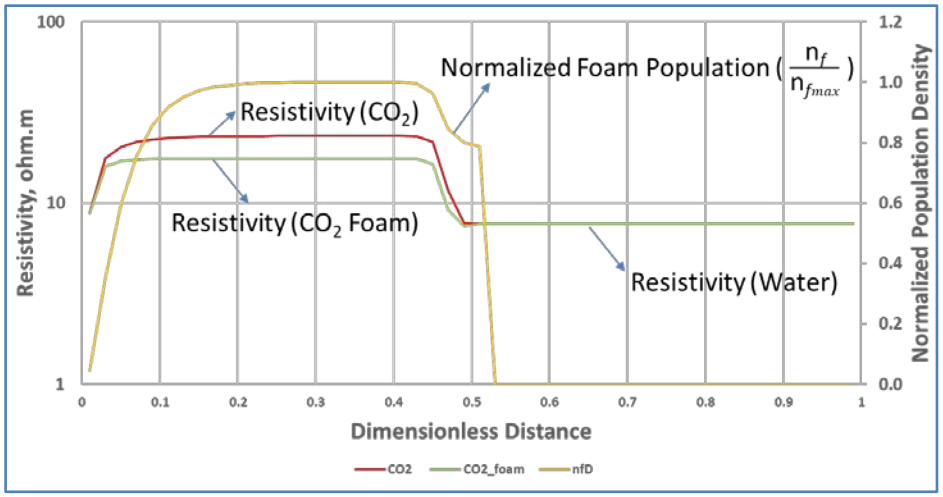

Fig. 6: Calculated resistivity profile during CO_2-Foam injection (PBE Solution).

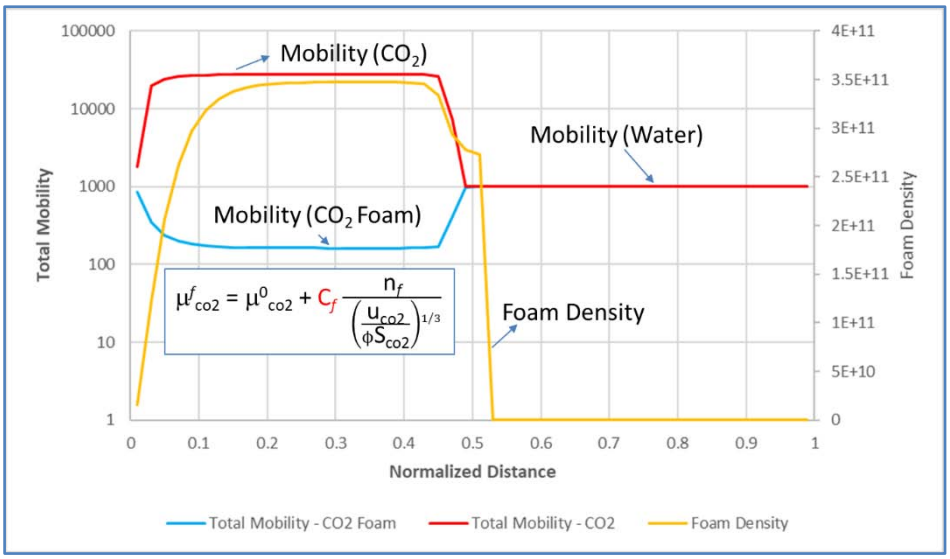

Fig. 7: Combined resistivity and mobility profile during CO_2-Foam injection (PBE Solution).

b) Resistivity Profiles – CO_2 Foam Displacement with Oil

The resistivity calculations for the CO_2 foam with oil were also made for CO_2-foam displacement with oil. For this model, the mobility effects were calculated using the steady-state assumption as outlined in Appendix A. The resistivity calculations were made assuming similar bulk conductivities as given in Table 2. The figures below show the calculated resistivity profiles for both ideal as well as non-ideal foam displacements:

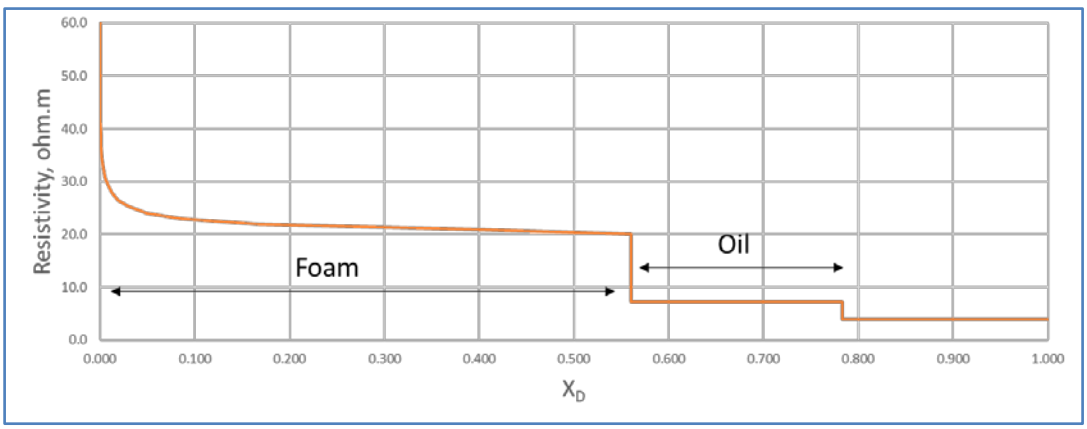

Fig. 8: Resistivity profile during ideal CO_2-Foam displacement.

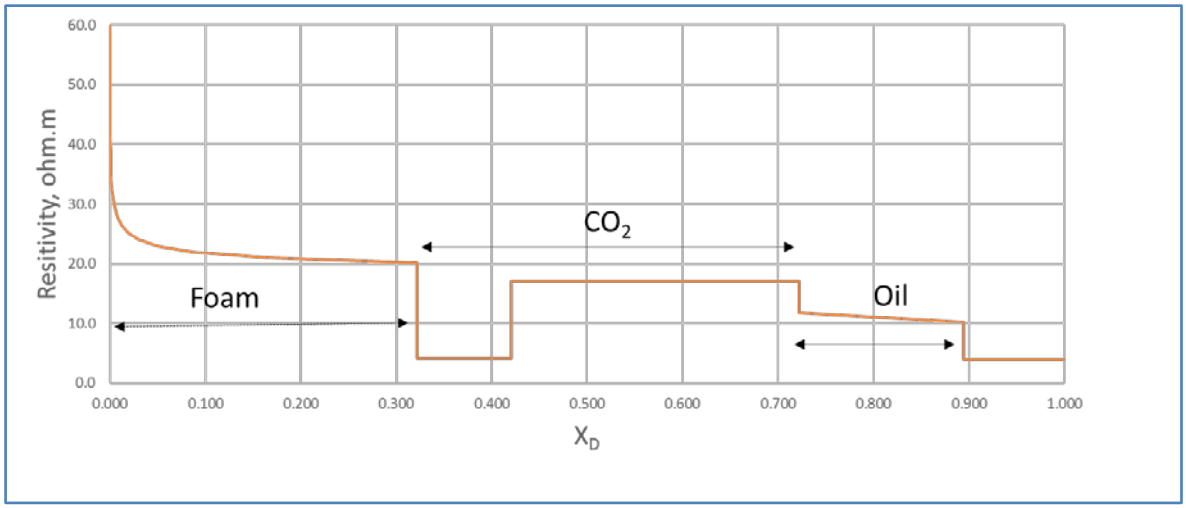

Fig. 9: Resistivity profile during non-deal CO_2-Foam displacement.

The figures below show the mobility distribution along with the resistivity profiles.

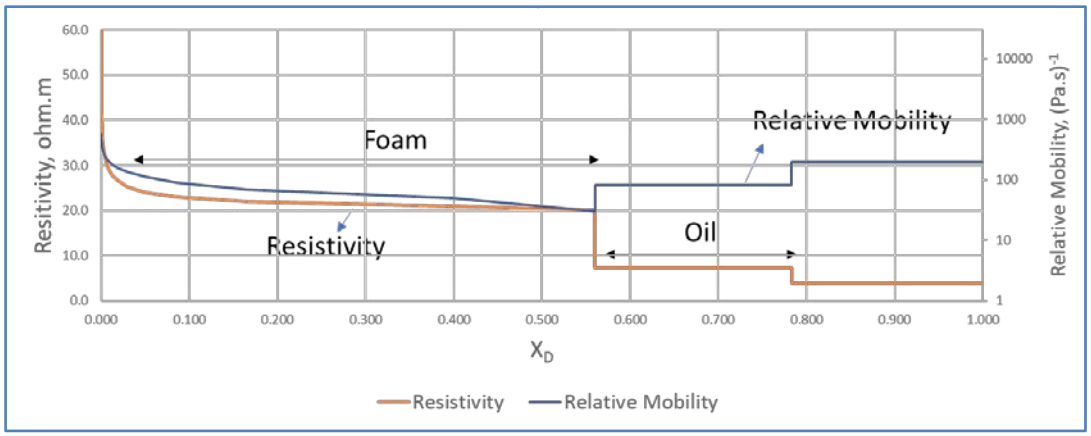

Fig. 10: Combined resistivity and mobility profile during CO_2-Foam injection (analytical Solution – ideal displacement).

As seen in Fig. 10, the resistivity profile during ideal displacement is like the PBE simulations shown earlier, and both models suggest a sharp resistivity contrast at the foam front. On the other hand, for non-ideal displacements, the resistivity profile is quite different. During these displacements, the resistivity profile, as shown in Fig. 11, indicate a staircase behavior, which extends into the miscible CO_2 bank.

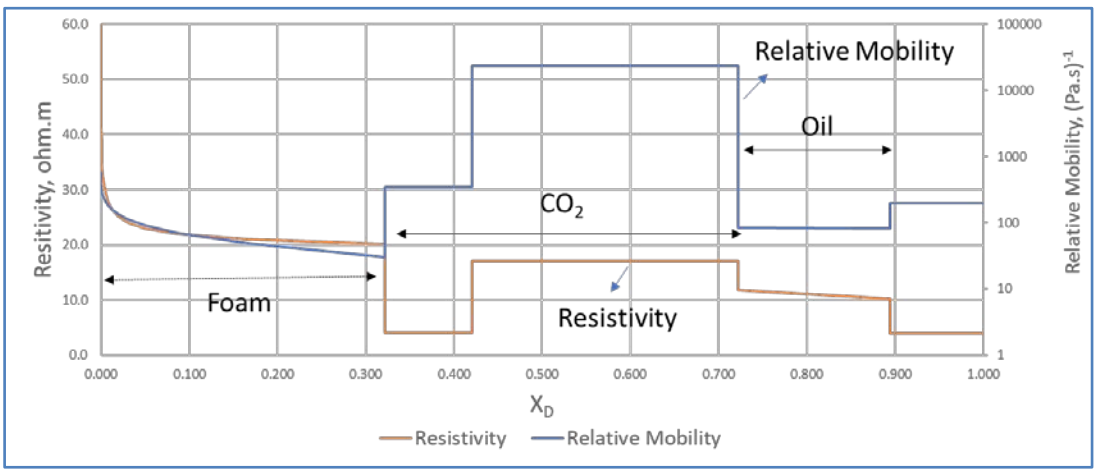

Fig. 11: Combined resistivity and mobility profile during CO_2-Foam injection (analytical solution – non-ideal displacement).

VI. Conclusions

In this paper, we presented a volumetric based foundation for resistivity and pressure monitoring during CO_2-foam displacements. Our results suggest that a combination of pressure and resistivity measurements in time-lapse mode could be deployed as an effective monitoring tool in field applications of the (CO_2) foam processes. The proposed method is novel as it could be employed to predict under-performing CO_2-foam floods and to improve oil recovery and CO_2 storage.

Other conclusions can be listed as follows:

- Pressure measurements during steady-state foam flow give rise to an ill-posed estimation problem and that grouping of foam parameters is necessary. For most reservoir applications, pressure measurements alone will not adequately describe the transient foam effects.
- Assuming brine in the reservoir, resistivity profiles during ideal CO_2 foam displacements should exhibit a distinctive signature at the foam front.
- During non-ideal CO_2 foam displacements, resistivity measurements by itself may not be enough to differentiate foam and miscible CO_2 banks. However, for these non-ideal cases, pressure measurements could be very utilized to locate these vastly contrasting mobility-fronts.

Acknowledgements

We would like to acknowledge financial support from Chevron for this research. We also acknowledge the input from Kurt Strack of KMS Technology.

Nomenclature

c_1 = a constant in the proposed foam conductivity model
C_c = a model parameter to represent foam coalescence
C_f = a model parameter to represent effective foam viscosity
C_g = a model parameter to represent foam generation
D = volumetric liquid fraction in the foam, fraction
d = value of determinant to capture the conditioning of the parameter estimation problem
epdry = a foam parameter used to capture the slope near critical water saturation
fmmob = a factor in steady-state foam model to represent the mobility factor
fmdry = a factor in steady-state foam model to represent the critical water saturation
epsurf = a steady-state foam parameter
f_{co2} = CO_2 phase fractional flow, fraction
f_w = water phase fractional flow, fraction
Fw = factor to capture the effect of water saturation on foam mobility reduction
K = bulk foam conductivity, (S/m)
k = permeability, m^2
k_{rCO2} = relative permeability to CO2 phase, fraction
k_{ro} = relative permeability to oil phase, fraction
k_{rw} = relative permeability to water phase, fraction
m = a model parameter for transient foam generation
M = measurement matrix
n = a model parameter for transient foam coalescence
R_{CO2} = resistivity of the CO_2 phase, ohm-m
R_f = resistivity of the foam, ohm-m
R_w = resistivity of water phase, ohm-m
n_f = foam texture or density, lamellae/unit volume
n_{fmax} = maximum foam density, lamellae/unit volume
r_c = foam (lamella) destruction rate
r_g = foam (lamella) generation rate
S = sensitivity matrix
S_{co2} = CO_2 saturation, fraction
S_o = oil saturation, fraction
S_w = water saturation, fraction
u_{co2} = CO_2 volumetric flux or superficial velocity, m/s
u_t = total velocity, m/s
u_w = water velocity, m/s
vf = volumetric fraction of rock and fluids, fraction
v_s = velocity of the foam front, m/s
v_w = velocity of the miscible (CO_2) front, m/s
X = vector defining the foam parameters
X_f = foam quality, fraction
μ_{co2}^{0} = CO_2 viscosity (without foam), Pa.s
μ_{co2}^{f} = effective viscosity of the CO_2 foam phase, Pa.s
ϕ = porosity, fraction
σ_{co2} = CO_2 conductivity (without foam), S/m
σ_{co2}^{f} = CO_2 conductivity (with foam), S/m
σ_f = foam conductivity, S/m
σ_w = water conductivity, S/m
∇p = total pressure gradient, Pa/m
∇p_w = pressure gradient for the water phase, Pa/m

References Références Referencias

1. Agnihotri, A.K. and Lemlich, R., 1981. Electrical conductivity and the distribution of liquid in polyhedral foam. Journal of Colloid and Interface Science, 84(1), pp.42-46.
2. Ashoori, E., van der Heijden, T., & Rossen, W. (2010, June 1). Fractional-Flow Theory of Foam Displacements with Oil. Society of Petroleum Engineers. doi:10.2118/121579-PA.
3. Berge, C., 2017. An Experimental Study of Foam Flow in Water Saturated Porous Media, MS thesis, University of Bergen, Bergen, Norway.
4. Bergmann, P., Ivandic, M., Norden, B., Rücker, C., Kiessling, D., Lüth, S., Schmidt-Hattenberger, C. and Juhlin, C., 2013. Combination of seismic reflection and constrained resistivity inversion with an application to 4D imaging of the CO2 storage site, Ketzin, Germany. Geophysics, 79(2), pp. B37-B50.
5. Bikerman, J.J., 2013. Foams (Vol. 10). Springer Science & Business Media.

6. Boerner, J. B., Volker, H., Repke, J. U. and Spitzer, 2015. The electrical conductivity of CO2-bearing pore waters at elevated pressure and temperature: a laboratory study and its implications in CO2 storage monitoring and leakage detection, *Geophys. J. Int.* (2015) 203, 1072–1084 doi: 10.1093/gji/ggv331.
7. Bouchedda, A. and Giroux, B., 2015, December. Synthetic Study of CO2 monitoring using Time-lapse Down-hole Magnetometric Resistivity at Field Reseach Station, Alberta, Canada. In 2015 SEG Annual Meeting. Society of Exploration Geophysicists.
8. Chang, Kin-Shiung, and Robert Lemlich. "A study of the electrical conductivity of foam." Journal of Colloid and Interface Science 73, no. 1 (1980): 224-232.
9. Christensen, N. B., D. Sherlock, and K. Dodds. "Monitoring CO2 injection with cross-hole electrical resistivity tomography." Exploration Geophysics 37.1 (2006): 44-49.
10. Cilliers, J.J., Wang, M. and Neethling, S.J., 1999. Measuring flowing foam density distributions using ERT. Ref, 5, pp.108-112.Clark, N. O. "The electrical conductivity of foam." Transactions of the Faraday Society 44 (1948): 13-15.
11. Cilliers, J.J., Xie, W., Neethling, S.J., Randall, E.W. and Wilkinson, A.J., 2001. Electrical resistance tomography using a bi-directional current pulse technique. Measurement Science and Technology, 12(8), p.997.
12. Dholkawala, Z.F., Sarma, H.K. and Kam, S.I., 2007. Application of fractional flow theory to foams in porous media. Journal of Petroleum Science and Engineering, 57(1-2), pp.152-165.
13. Feitosa, K., Marze, S., Saint-Jalmes, A. and Durian, D.J., 2005. Electrical conductivity of dispersions: from dry foams to dilute suspensions. Journal of Physics: Condensed Matter, 17(41), p.6301.
14. Ferno, M. A., Gauteplass, J., Pancharoen, M., Haugen, A., Graue, A., Kovscek, A. R., & Hirasaki, G. J. (2014, October 27). Experimental Study of Foam Generation, Sweep Efficiency and Flow in a Fracture Network. Society of Petroleum Engineers. doi:10.2118/170840-MS.
15. Gargar, N.K., Mahani, H., Rehling, J.G., Vincent-Bonnieu, S., Kechut, N.I. and Farajzadeh, R., 2015, April. Fall-Off Test Analysis and Transient Pressure Behavior in Foam Flooding. In IOR 2015-18th European Symposium on Improved Oil Recovery.
16. Haroun, M., Mohammed, A.M., Somra, B., Punjabi, S., Temitope, A., Yim, Y., Anastasiou, S., Baker, J.A., Haoge, L., Al Kobaisi, Aminzadeh, F., M., Karakas, M., Corova, F. (2017, November 13). Real-Time Resistivity Monitoring Tool for In-Situ Foam Front Tracking. Society of Petroleum Engineers. doi:10.2118/188391-MS.
17. Hirasaki, G.J. and Lawson, J.B., 1985. Mechanisms of foam flow in porous media: apparent viscosity in smooth capillaries. Society of Petroleum Engineers Journal, 25(02), pp.176-190.
18. Kam, S.I., 2008. Improved mechanistic foam simulation with foam catastrophe theory. Colloids and Surfaces A: Physicochemical and Engineering Aspects, 318(1-3), pp.62-77.
19. Kam, S.I., Nguyen, Q.P., Li, Q. and Rossen, W.R., 2007. Dynamic simulations with an improved model for foam generation. SPE Journal, 12(01), pp.35-48.
20. Karakas, M. and Aminzadeh, F., 2017, Optimization of CO_2-Foam Injection through Resistivity and Pressure Measurements, Provisional US Patent Application, Serial No. 62/511,547.
21. Kiessling, D., Schmidt-Hattenberger, C., Schuett, H., Schilling, F., Krueger, K., Schoebel, B., Danckwardt, E., Kummerow, J. and CO2SINK Group, 2010. Geoelectrical methods for monitoring geological CO2 storage: first results from cross-hole and surface–downhole measurements from the CO2SINK test site at Ketzin (Germany). International Journal of Greenhouse Gas Control, 4(5), pp.816-826.
22. Kim, J., Dong, Y., & Rossen, W. R. (2005, December 1). Steady-State Flow Behavior of CO2 Foam. Society of Petroleum Engineers. doi:10.2118/89351-PA.
23. Kim, J., Nam, M.J. and Matsuoka, T., 2016. Monitoring CO2 drainage and imbibition in a heterogeneous sandstone using both seismic velocity and electrical resistivity measurements. Exploration Geophysics, 47(1), pp.24-31.
24. Kim, J. W., Xue, Z., & Matsuoka, T. (2010, January 1). Experimental Study On CO2 Monitroing and Saturation With Combined P-wave Velocity and Resistivity. Society of Petroleum Engineers. doi:10.2118/130284-MS.
25. Kovscek, A.R. and Radke, C.J., 1994. Fundamentals of foam transport in porous media.
26. Kovscek, A.R., Patzek, T.W. and Radke, C.J., 1995. A mechanistic population balance model for transient and steady-state foam flow in Boise sandstone. Chemical Engineering Science, 50(23), pp.3783-3799.
27. Kuuskraa, V.A. and Koperna, G.J., 2006. Evaluating the potential for 'game changer' improvements in oil recovery efficiency from CO2 enhanced oil recovery. Prepared for US Department of Energy, Office of Fossil Energy—Office of Oil and Natural Gas.
28. Lemlich, R., 1985. Semitheoretical equation to relate conductivity to volumetric foam density. Industrial & Engineering Chemistry Process Design and Development, 24(3), pp.686-687.
29. Lotfollahi, M., Farajzadeh, R., Delshad, M., Varavei, A., & Rossen, W. R. (2016, March 21). Comparison of Implicit-Texture and Population-Balance Foam

Models. Society of Petroleum Engineers. doi:10.2118/179808-MS.
30. Ma, K., Ren, G., Mateen, K., Morel, D., & Cordelier, P. (2015, June 1). Modeling Techniques for Foam Flow in Porous Media. Society of Petroleum Engineers. doi:10.2118/169104-PA.
31. Mahani, H., Sorop, T., van den Hoek, P., Brooks, D., & Zwaan, M. (2011, January 1). Injection Fall-Off Analysis of Polymer flooding EOR. Society of Petroleum Engineers. doi:10.2118/145125-MS.
32. Montaron, B. (2009, April 1). Connectivity Theory – A New Approach to Modeling Non-Archie Rocks. Society of Petrophysicists and Well-Log Analysts.
33. Nakatsuka, Y., Xue, Z., Garcia, H. and Matsuoka, T., 2010. Experimental study on CO2 monitoring and quantification of stored CO2 in saline formations using resistivity measurements. International Journal of Greenhouse Gas Control, 4(2), pp.209-216.
34. Namdar Zanganeh, M., & Rossen, W. (2013, January 30). Optimization of Foam Enhanced Oil Recovery: Balancing Sweep and Injectivity. Society of Petroleum Engineers. doi:10.2118/163109-PA.
35. Nguyen, Q., Hirasaki, G., & Johnston, K. (2015). Novel CO2 Foam Concepts and Injection Schemes for Improving CO2 Sweep Efficiency in Sandstone and Carbonate Hydrocarbon Formations. Univ. of Texas, Austin, TX (United States).
36. Omar, S., Jaafar, M. Z., Ismail, A. R., & Wan Sulaiman, W. R. (2013, July 2). Monitoring Foam Stability in Foam Assisted Water Alternate Gas (FAWAG) Processes Using Electrokinetic Signals. Society of Petroleum Engineers. doi:10.2118/165312-MS.
37. Onishi, K., Ishikawa, Y., Yamada, Y. and Matsuoka, T., 2006, January. Measuring electric resistivity of rock specimens injected with gas, liquid and supercritical CO2. In 2006 SEG Annual Meeting. Society of Exploration Geophysicists.
38. Passalacqua, H., S. Davydycheva, and K. Strack, 2018, Feasibility of multi-physics reservoir monitoring for Heavy Oil, Heavy Oil Conference Kuwait, SPE-193690-MS, doi: 10.2118/193690-MS.
39. Prigiobbe, Valentina, et al. "Transport of Nanoparticle-Stabilized CO_2-Foam in Porous Media." Transport in Porous Media 111.1 (2016): 265-285.
40. Schmidt-Hattenberger, C., Bergmann, P., Labitzke, T. and Wagner, F., 2014. CO2 migration monitoring by means of electrical resistivity tomography (ERT)–Review on five years of operation of a permanent ERT system at the Ketzin pilot site. Energy Procedia, 63, pp.4366-4373.
41. Strack, K. M., Hinojosa, H., Lüschen, E., and Martinez, Y., 2022, Using Electromagnetics for Geothermal and Carbon Capture, Utilization and Storage (CCUS) applications, European Geothermal Congress, Berlin, Germany | 17-21 October 2022, www.europeangeothermalcongress.eu
42. Strack, K.-M., 2014, Future directions of Electromagnetic Methods for Hydrocarbon Applications, Surveys in Geophysics, 35, 157-177, doi:10.1007/s10712-013-9237-z.)
43. Tapp, H.S., Peyton, A.J., Kemsley, E.K. and Wilson, R.H., 2003. Chemical engineering applications of electrical process tomography. Sensors and Actuators B: Chemical, 92(1-2) pp.17-24.
44. Wang, M. and Cilliers, J.J., 1999. Detecting non-uniform foam density using electrical resistance tomography. Chemical Engineering Science, 54(5), pp.707-712.
45. Wu, Y., Hubbard, S. and Wellman, D., 2012. Geophysical monitoring of foam used to deliver remediation treatments within the vadose zone. Vadose Zone Journal, 11(4).
46. Xue, Z., Kim, J. W., Mito, S., Kitamura, K., & Matsuoka, T., 2009, Detecting and Monitoring CO2 With P-Wave Velocity and Resistivity from both Laboratory and Field Scales. Society of Petroleum Engineers. doi:10.2118/126885-MS.

Appendix A – Analytical Solution

In the example provided by Ashoori et al. (2010), the following fluid and rock parameters are assumed:

Table A1: Model Parameters used for Analytical Simulations

μ_w	0.001	Pa.s
μo	0.005	Pa.s
μg	2E-05	Pa.s
ϕ	0.25	
S_{gr}	0.1	
S_{wc}	0.1	
S_{or}	0.1	

Water and Oil phase relative permeabilities are modeled as follows:

$$k_{rw}=0.20*((S_w-0.1)/0.8)^{4.2} \text{ (Water)} \quad \text{(A1)}$$

$$k_{ro}=0.94*((1-S_w-0.1)/0.8)^{1.3} \text{ (Oil)} \quad \text{(A2)}$$

Water and CO_2 phase relative permeabilities are represented by the following relationships:

$$k_{rw}=0.20*((S_w-0.1)/0.8)^{4.2} \text{ (Water)} \quad \text{(A3)}$$

$$k_{rg}{}^{0} = 0.94*((1-S_w-0.1)/0.8)^{1.3} \text{ (CO_2 without foam)} \quad \text{(A4)}$$

In these models, foam reduces the CO_2 relative permeability, using the steady-state assumptions, as follows:

$$k_{rg}^{f} = k_{rCg}^{0} * \frac{1}{1+fmmob * Fwater} \quad (A5)$$

Where:

$$F_{water} = 0.5 + \pi^{-1} tan^{-1}[epdry(Sw - fmdry)] \quad (A6)$$

where fmdry and epdry are empirical parameters based on experimental data.

In the example by Ashoori et al., 2010, the following parameters were utilized:

Table A2: Foam Parameters used for Analytical Simulations

fmmob	55000
fmdry	0.316
epdry	1000
epsurf	100

Using these parameters, fractional flow curves for foam/water, CO_2/water and oil/water phases were reconstructed. Also, we used the two separate solutions; the first solution assumes an ideal displacement where the miscible fronts and the surfactant (foam) fronts travel at the same speed. For this to happen, there must be a minimal Surfactant adsorption as well as very favorable partitioning of the surfactant into the CO_2 phase. In the ideal displacement case, the solution paths are constructed by first drawing a tangent from the M=D=(1,1) point to the curve representing the fractional flow of foam, as shown in the figure below:

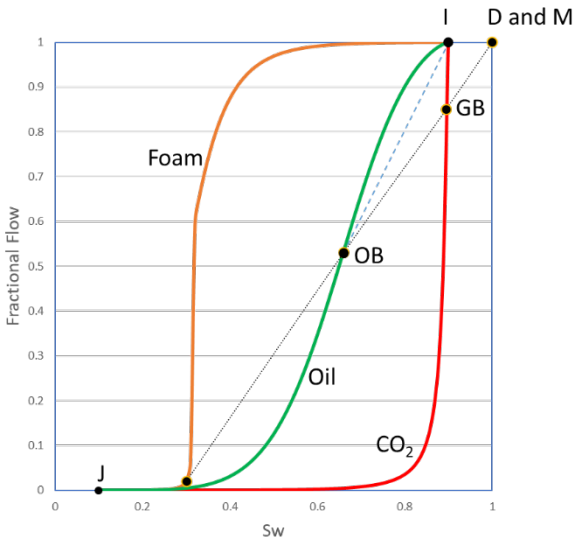

Fig. A1: Fractional flow – Ideal Displacement.

The saturation profile for the ideal displacement case is as follows:

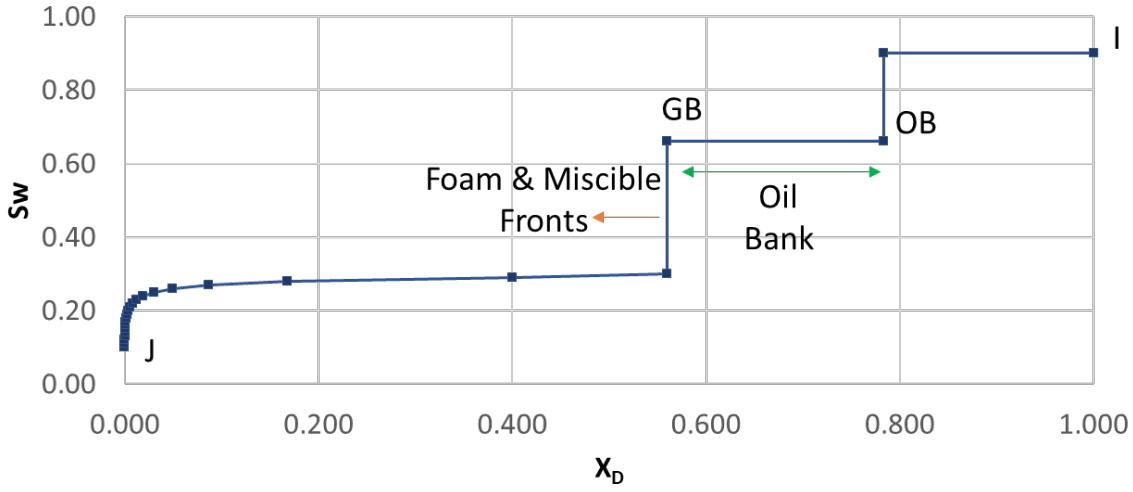

Fig. A2: Saturation profile – Ideal Displacement.

The second solution is non-ideal displacement where the miscible fronts and the surfactant (foam) fronts travel at different speeds. In this case, the surfactant adsorption as well as partitioning of the surfactant into the water phase slows down the speed of the foam (surfactant) front. On the other hand, the miscible (CO_2) front moves at the same speed as before. Therefore, miscible front shoots ahead of the foam (surfactant) front. Thus, a CO_2 bank forms. In this case, there are four different banks, and the construction of the solution paths starts first by drawing tangents from point D and the miscibility point, point M (1,1) to curves representing the fractional flow of oil and foam, respectively.

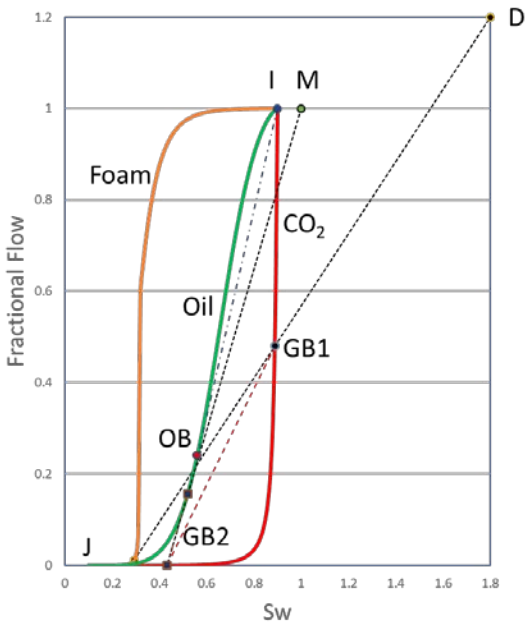

Fig. A3: Fractional flow, Non-Ideal displacement.

The saturation profile for the non-ideal displacement case is as follows:

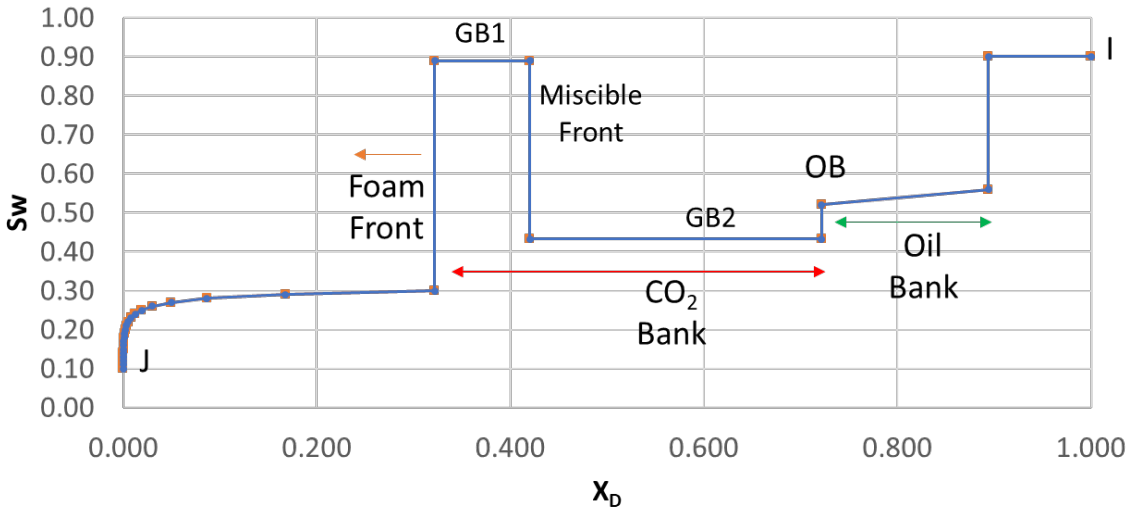

Fig. A4: Saturation profile, Non-Ideal displacement.

Appendix B – Population based Foam Model

Assuming one-dimensional flow of water and CO_2, the material balance of water is described by the following equation:

$$\phi \frac{\partial S_w}{\partial t} + u_t \frac{\partial f_w}{\partial x} = 0 \qquad \text{(B1)}$$

In this model, total flow rate (u_t) is assumed to be constant. As usual, water fractional flow is written as follows:

$$f_w = \frac{\frac{k_{rw}}{\mu_w}}{\frac{k_{rw}}{\mu_w} + \frac{k_{rco2}}{\mu^f_{co2}}} \qquad \text{(B2)}$$

where μ^f_{co2} is the CO_2– Foam viscosity and is given by (Hirasaki et al. 1985)

$$\mu^f_{co2} = \mu^0_{co2} + C_f \frac{n_f}{(\frac{u_{co2}}{\phi S_{co2}})^{1/3}} \qquad \text{(B3)}$$

In this equation, C_f is an empirical parameter based on experimental data.

Foam density ((n_f) equation is described by the following equation (Kovscek et al. 1995):

$$\phi \frac{\partial (S_{co2} n_f)}{\partial t} + u_t \frac{\partial (f_{co2} n_f)}{\partial x} = \varphi S_{co2} (r_g - r_c) \quad \text{(B4)}$$

The rate of foam generation is given by

$$r_g = C_g \nabla p^m \quad \text{(B5)}$$

and the rate of foam coalescence is given by

$$r_c = C_c n_f \left(\frac{S_w}{S_w - S_w^*}\right)^n \quad \text{(B6)}$$

Where C_g, C_c, m and n are model parameters. S_w^* is the water saturation linked with the critical capillary pressure for a foam–water system. In high permeability reservoirs, S_w^* is expected to be small. Also, the foam behavior around the critical water saturation could be quite abrupt.

The water rate is given by

$$u_w = - \frac{k\, k_{rw}}{\mu_w} \nabla p_w \quad \text{(B7)}$$

and the foam rate is given by:

$$u_{co2} = - \frac{k\, k_{rco2}}{\mu^o_{co2}} (\nabla p_w - \nabla p_c) \quad \text{(B8)}$$

At steady state conditions, the foam generation rate is equal to the foam destruction (or coalescence) rate.

$$r_g = r_c \quad \text{(B9)}$$

when this relationship is inserted into the foam-viscosity equation:

$$\mu^f_{co2} = \mu^0_{co2} + C_f \frac{n_f}{(\frac{u_{co2}}{\phi S_{co2}})^{\frac{1}{3}}} \quad \text{(B10)}$$

the following relationship is obtained, representing the foam viscosity:

$$\mu^f_{co2} = \mu^0_{co2} + \frac{C_g C_f}{C_c} \frac{\nabla p^m}{(\frac{S_w}{S_w - S_w^*})^n (\frac{u_{co2}}{\phi S_{co2}})^{\frac{1}{3}}} \quad \text{(B11)}$$

Appendix C - Sensitivity Coefficients

For a single-measurement (pressure) case, the Model response is defined as follows:

$$M(X) = \nabla p_{mod} (\bar{X}) \quad \text{(C1)}$$

Where M is a matrix representing the model response and X is a vector representing the system unknowns:

$$X = \text{foam parameters } [X_1, X_2, X_3, \ldots X_i \ldots, X_p] \quad \text{(C2)}$$

where p is the total number of unknows. In this case, the Sensitivity Coefficients are defined as follows:

$$S(X) = [\nabla_x M^T(X)] \quad \text{(C3)}$$

and the Sensitivity Matrix for the Single Response Case is defined as follows:

$$S = \begin{bmatrix} M_{11} \ldots\ldots\ldots\ldots M_{1p} \\ M_{k1} \ldots\ldots\ldots\ldots M_{kp} \end{bmatrix} \quad \text{(C4)}$$

or

$$S = \begin{bmatrix} \frac{\delta M_1}{\delta x_1} \ldots\ldots\ldots \frac{\delta M_1}{\delta x_p} \\ \frac{\delta M_k}{\delta x_1} \ldots\ldots\ldots \frac{\delta M_k}{\delta x_p} \end{bmatrix} \quad \text{(C5)}$$

where k is the number of measurements. Sensitivity of the Model response (M_i) to parameter vector X_j is defined as follows:

$$S^{(l)}_{ij} = \frac{\delta M_i}{\delta x_j} \Big|_{x^{(l)}} \quad \text{(C6)}$$

where $X^{(l)}$ represents the parameter vector which was used in generating the forward simulations.

Appendix D – Conductivity of Fluid Mixtures

Conductivity of fluid mixtures in porous media can be represented using the mixing law (Montaron, B., 2009). For a rock saturated with fluids, the total conductivity is expressed by the following equation:

$$\sigma^{1/2} = vf_1 \sigma_1^{1/2} + vf_2 \sigma_2^{1/2} + vf_3 \sigma_3^{1/2} \quad \text{(D1)}$$

where σ_i and vf_i represent the conductivity and the volumetric fraction of each component (rock and fluid), respectively. Additionally, the total volumetric fraction can be written as:

$$vf_1 + vf_2 + vf_3 = 1.0 \quad \text{(D2)}$$

for a water and oil/gas/CO_2 system these relationships become:

$$\sigma_1 = \sigma_R = 0, \qquad vf_1 = 1 - \phi \quad \text{(D3)}$$

$$\sigma_2 = \sigma_o = 0, \qquad vf_2 = S_o \phi \quad \text{(D4)}$$

$$\sigma_3 = \sigma_w, \qquad vf_3 = \sigma_w \phi \quad \text{(D5)}$$

and using the mixing law, we obtain:

$$\sigma = \sigma_w (S_w \phi)^2 \quad \text{(D6)}$$

This result is similar to Archie's law:

$$\sigma = \frac{\sigma_w S_w^n \phi^m}{a} \quad \text{(D7)}$$

where a, n and m are constants. For a CO_2-Foam and water system, the mixing law equations become:

$$\sigma_1 = \sigma_R = 0, \qquad vf_1 = 1 - \phi \quad \text{(D8)}$$

$$\sigma_2 = \sigma_f, \qquad vf_2 = S_{co2}^f \phi \quad \text{(D9)}$$

$$\sigma_3 = \sigma_w, \qquad vf_3 = \sigma_w \phi \quad \text{(D10)}$$

and finally:

$$\sigma = \phi^2 [S_{co2}^f \sigma_f^{1/2} + S_w \sigma_w^{1/2}]^2 \quad \text{(D11)}$$